2021 43rd Annual International Conference of the
IEEE Engineering in Medicine & Biology Society (EMBC)
Oct 31 - Nov 4, 2021. Virtual Conference

2021 43rd Annual International Conference of the IEEE Engineering in Medicine & Biology Society (EMBC) | 978-1-7281-1179-7/21/$31.00 ©2021 IEEE | DOI: 10.1109/EMBC46164.2021.9630653

Machine learning-based distinction of left and right foot contacts in lower back inertial sensor gait data

Martin Ullrich[1], Arne Küderle[1], Luca Reggi[2], Andrea Cereatti[3], Bjoern M. Eskofier[1], and Felix Kluge[1]

Abstract— **Digital gait measures derived from wearable inertial sensors have been shown to support the treatment of patients with motor impairments. From a technical perspective, the detection of left and right initial foot contacts (ICs) is essential for the computation of stride-by-stride outcome measures including gait asymmetry. However, in a majority of studies only one sensor close to the center of mass is used, complicating the assignment of detected ICs to the respective foot. Therefore, we developed an algorithm including supervised machine learning (ML) models for the robust classification of left and right ICs using multiple features from the gyroscope located at the lower back. The approach was tested on a data set including 40 participants (ten healthy controls, ten hemiparetic, ten Parkinson's disease, and ten Huntington's disease patients) and reached an accuracy of 96.3% for the overall data set and up to 100.0% for the Parkinson's sub data set. These results were compared to a state-of-the-art algorithm. The ML approaches outperformed this traditional algorithm in all subgroups. Our study contributes to an improved classification of left and right ICs in inertial sensor signals recorded at the lower back and thus enables a reliable computation of clinically relevant mobility measures.**

I. Introduction

The objective analysis of gait using wearable sensor systems is gaining importance in the treatment of patients with motor impairments [1]. Various studies have identified gait parameters captured by wearable inertial measurement units (IMUs) as digital measures for gait performance in different diseases like Parkinson's disease (PD), Huntington's disease (HD), and post-stroke Hemiparesis (HE) [2]–[4].

From a technical perspective, an important aspect in the signal processing pipeline for IMU-based gait analysis is the segmentation of the recorded data into meaningful portions. One basic unit of gait measurements is a stride, which describes the period from the initial foot contact (IC) of one foot until the next IC of the same foot in a gait cycle [5]. Stride-level information is for example essential for defining walking bouts [6], [7], the measurement of gait variability [8], or the computation of gait asymmetry [9], where differences between left and right strides are investigated.

In their review about the use of wearable motion sensors for gait assessment, Brognara et al. reported that a majority of studies prefers the use of only one single sensor unit, which is most often attached close to the center of mass of the participant (e.g. on the lower back) [10]. For this sensor setup, the detection of ICs is very well investigated [11]–[14]. Still, to convert a sequence of ICs into strides according to the definition given above, ICs of the same foot need to be grouped and hence the laterality of each IC must me determined. However, this information is usually not directly available from IC detection algorithms and, therefore, stride segmentation is not trivial. Breaks, turns or missed ICs in the detection contradict the assumption of a steady alternating sequence of left and right ICs. Thus, only the explicit determination of the laterality of the ICs allows to define stride borders and additionally enable to differentiate between left and right strides which is, for example, crucial for the investigation of gait asymmetry.

To the best of our knowledge, there is only one publication describing an approach for the distinction of left and right ICs detected from a lower back-mounted sensor: McCamley et al. used the sign (positive or negative) of the lowpass filtered gyroscope signal of the vertical axis at the sample of the detected IC to determine the foot it was performed with [11]. However, the laterality assignment was not separately evaluated in their article. Furthermore, only young and healthy participants took part in their study and the transferability to patients with movement disorders and thus potentially higher gait variability needs to be investigated.

Considering the high relevance of stride level parameters, the left-right distinction is a crucial part of a lower back sensor-based gait analysis pipeline and needs further investigations, given the lack of suitable well evaluated algorithms. Therefore, the goal of this study is twofold: First, we propose potential improvements for the algorithm by McCamley et al. and evaluate the algorithm on data from patients with movement disorders. Second, we present a new approach for the left-right distinction based on supervised machine learning (ML) including a cross-validation. For the experiments, a data set including 40 participants with and without movement impairments, that was previously recorded and presented by Trojaniello et al. [15], was analyzed. The results of our study contribute to a better understanding and an increased reliability of stride-based gait analysis in single-sensor settings.

II. Methods

A. Data set

The data set contained four groups (healthy controls (HC), patients with Parkinsons disease (PD), patients with Huntington's disease (HD), and hemiparetic patients (HE))

[1]Machine Learning and Data Analytics Lab, Friedrich-Alexander-Universität Erlangen-Nurnberg (FAU), Erlangen, Germany (e-mail: martin.ullrich@fau.de, arne.kuederle@fau.de, bjoern.eskofier@fau.de, felix.kluge@fau.de).

[2]Department of Electronics and Telecommunications, Politecnico di Torino, Torino, Italy (e-mail: andrea.cereatti@polito.it).

[3]Health Sciences and Technologies (CIRI-SDV), University of Bologna, Bologna, Italy (e-mail: luca.reggi2@unibo.it).

Authorized licensed use limited to: Norges Teknisk-Naturvitenskapelige Universitet. Downloaded on July 14,2022 at 10:45:38 UTC from IEEE Xplore. Restrictions apply.

TABLE I

DEMOGRAPHIC DATA, GIVEN IN MEAN (SD). A DETAILED DESCRIPTION OF THE DATA SET IS PRESENTED IN [15].

	All	***HC***	***PD***	***HD***	***HE***
Disease severity	-	-	34.9[a] (16.9)	62.7[b] (19.1)	3.3[c] (1.5)
Age [yrs]	63.6 (12.7)	69.7 (5.8)	73.8 (5.7)	52.2 (13.6)	58.7 (12.1)
Height [cm]	166 (7)	162 (7)	166 (10)	166 (8)	172 (6)
Mass [kg]	68.7 (13.0)	63.6 (5.7)	67.7 (9.3)	61.5 (11.2)	82.1 (17.2)
Sex [m / f]	21 / 19	4 / 6	5 / 5	5 / 5	7 / 3

[a]Unified Parkinsons Disease Rating Scale (UPDRS)
[b]Unified Huntingtons Disease Rating Scale (UHDRS)
[c]Functional Ambulatory Category (FAC)

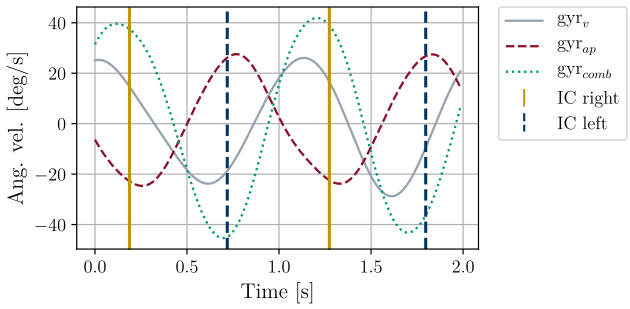

Fig. 1. Example signal window with the bandpass filtered gyr$_v$ and gyr$_{ap}$ signals, as well as the combined gyr$_{comb}$ signal. The left and right ICs are displayed as vertical lines based on the gold standard data.

with ten participants each (Table I) [15]. The data set was analyzed as a whole, but also subdivided based on the groups. In total, this resulted in five data sets that were investigated separately and will be called *All*, *HC*, *PD*, *HD*, and *HE* in the following.

For the data acquisition, participants were equipped with an IMU (Opal, APDM Inc., Portland, OR, USA) attached on the lower back, including a 3-axis accelerometer and a 3-axis gyroscope recording at 128 Hz. A 7 m long instrumented mat (GAITRite Electronic Walkway, CIR Systems Inc., Franklin, NJ, USA) was used to acquire reference data with a sampling rate of 120 Hz. The sensor and the mat were synchronized and only the data recorded during the passes on the mat were considered. All participants performed straight walking back and forth at comfortable and at higher speed for one minute each along a 12-meter walkway with the instrumented mat placed centrally in the area between the turning points [15].

The true time points and *left-right* labels for all ICs were available from the instrumented mat. They served as ground truth label for the training and the evaluation of the algorithms as described in the following. The IC time points for this study were used from the ground truth which allowed the isolation of the task of laterality assignment.

B. McCamley Algorithm and Extensions

In the algorithm by McCamley et al., the gyroscope signal of the vertical axis (gyr$_v$) is used to differentiate left and right ICs [11]. In a pre-processing step, the signal mean is subtracted and a lowpass filter (4th order Butterworth filter with 2 Hz cutoff frequency) is applied. Afterwards, the sign of the filtered gyr$_v$ value at the IC time point n is considered: In case of a positive value of gyr$_v$[IC$_n$], the IC is assigned to the right foot and in case of a negative value it is assigned to the left foot. The filtered gyr$_v$ signal is suitable, as it behaves like a periodic wave alternating between left and right ICs (Fig. 1).

Additionally, we observed the gyroscope signal of the anterior-posterior axis (gyr$_{ap}$) to behave similarly periodic with a constant phase shift w.r.t. gyr$_v$ after application of the lowpass filter described above. Therefore, it is also a suitable input signal for the McCamley algorithm, when inverting the sign (Fig. 1). As a third potential input signal, a combination of the filtered signals from the vertical and the anterior-posterior signals, gyr$_{comb}$, was computed by subtracting the filtered gyr$_{ap}$ signal from the filtered gyr$_v$ signal with the goal to enhance the sinusoidal shape of the signal and improve the robustness of the laterality assignment based on the sign (Fig. 1):

$$\text{gyr}_{comb} = \text{gyr}_v - \text{gyr}_{ap}$$

C. Machine Learning Approaches

1) Feature extraction: Based on the algorithm of McCamley et al., a set of features was extracted from the filtered gyr$_v$ and gyr$_{ap}$ signals. Additionally to the filtered raw signal values (gyr$_{v/ap}$[IC$_n$]), we calculated the first and second derivative (g$\dot{\text{y}}$r$_{v/ap}$[IC$_n$] and g$\ddot{\text{y}}$r$_{v/ap}$[IC$_n$], respectively) at the time points of the individual n ICs. For a total number of N ICs in the data set, this resulted in a $N \times 6$ feature matrix. Each feature was min-max-normalized to the range of $[0, 1]$. The ground truth labels for each IC (*left* or *right*) were provided by the gold standard data.

2) Classification: In the context of ML, the left-right distinction is essentially a binary classification. We tested four ML approaches for this task: Support Vector Machines with linear and radial basis function kernel (SVM-lin, SVM-rbf), k-Nearest-Neighbors (kNN), and Random Forest Classifiers (RFC). All classifiers were implemented using Python (version 3.7) and scikit-learn (version 0.23.1) [16].

The classifiers were evaluated in individual leave-one-participant-out cross-validations for the entire data set as well as for the respective sub sets. An inner 5-fold cross validation with grid search (for SVM-lin, SVM-rbf, and kNN) or randomized search (for RFC) was performed to find optimized training parameters within a standard parameter space [17]. For the outer and the inner cross-validation, the accuracy was used as the optimization target parameter.

The accuracy was computed by counting the number of agreements between predicted *left* and *right* labels and the ground truth labels and dividing it over the total number of ICs:

$$accuracy = \frac{\sum_{n=1}^{N} pred_n == true_n}{N}$$

Authorized licensed use limited to: Norges Teknisk-Naturvitenskapelige Universitet. Downloaded on July 14,2022 at 10:45:38 UTC from IEEE Xplore. Restrictions apply.

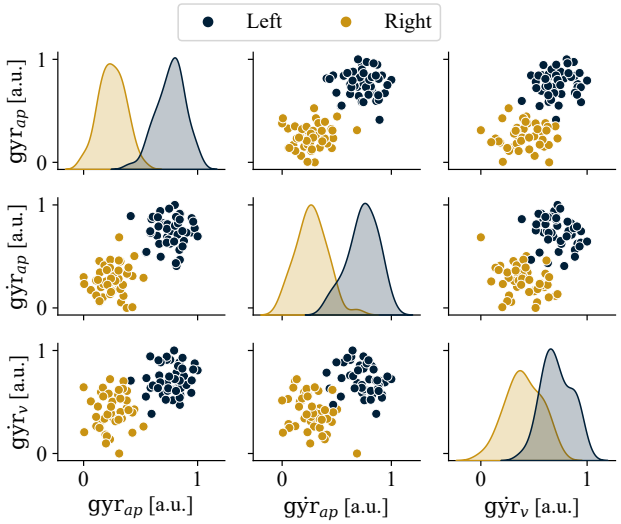

Fig. 2. Pair plot showing an excerpt of three features for one participant from the *HD* subgroup. On the diagonal, the distribution of the individual features are shown for left and right ICs. The distributions of the respective pairs of those features are presented on the crossing positions in the figure.

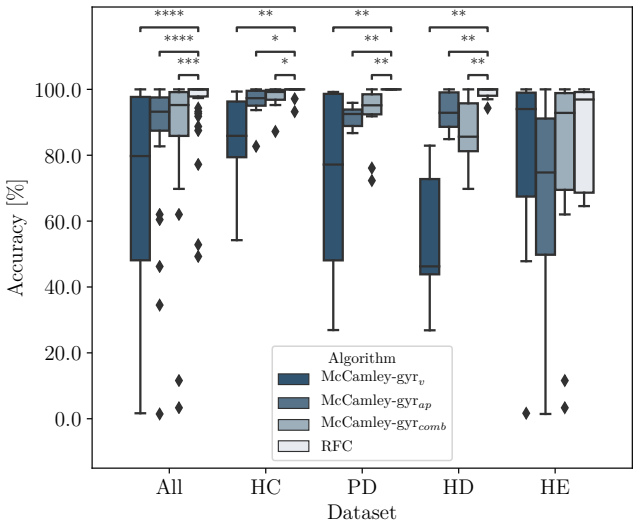

Fig. 3. Boxplots for the classification accuracy of the different approaches based on McCamley et al. and RFC as a representative example for the ML algorithms. Significant differences were identified using Wilcoxon signed-rank tests with *: $p \leq 0.05$, **: $p \leq 0.01$, ***: $p \leq 0.001$, ****: $p \leq 0.0001$.

D. Comparative analysis

In order to compare the performances of the different approaches, statistical tests were performed. The non-normally distributed accuracy values of the cross-validations of the different McCamley configurations and the ML approaches were compared using Wilcoxon signed-rank tests.

III. Results

In total, 4377 ICs (*HC*: 1185, *PD*: 1187, *HD*: 1066, *HE*: 939) were available in the data set. An excerpt of the feature space is shown for one participant in Fig. 2. Overall, the best performance was achieved for the *PD* sub data set and the RFC with a mean accuracy of 100.0% in the leave-one-participant-out cross-validation (Table II). There was no clear tendency regarding the performance of different input signals between sub data sets in the McCamley results. Each gyr$_v$, gyr$_{ap}$ and gyr$_{comb}$ at least once performed best for one of the sub data sets. For all sub data sets, except for *HE*, the ML approaches reached a significantly higher mean accuracy than the McCamley approaches (exemplarily shown for RFC in Fig. 3). In general, the ML approaches tended to show a smaller interquartile range (IQR) than the McCamley approaches over the cross-validation.

IV. Discussion

In this study, we investigated ML-based algorithms for the distinction of left and right ICs from inertial sensor data measured at the lower back. The pre-processing and the feature extraction were based on the work of McCamley et al. [11], who proposed an algorithm based on thresholding of one single gyroscope axis (gyr$_v$). We also expanded the approach by McCamley et al. by two other signal configurations (gyr$_{ap}$, gyr$_{comb}$) and performed comparisons between the approaches.

TABLE II

Classification accuracy given as mean values (interquartile range) of cross-validation in %)

	All	***HC***	***PD***	***HD***	***HE***
McCamley-gyr$_v$	72.0 (49.6)	84.9 (16.9)	70.7 (50.5)	54.2 (28.9)	78.0 (31.5)
McCamley-gyr$_{ap}$	87.1 (10.1)	96.1 (4.5)	91.6 (5.0)	93.2 (10.5)	67.3 (41.4)
McCamley-gyr$_{comb}$	87.9 (13.3)	97.5 (3.0)	92.1 (6.1)	87.0 (14.5)	75.2 (29.4)
SVM-lin	96.1 (2.2)	99.3 (0.0)	99.9 (0.0)	99.0 (0.8)	79.6 (40.1)
SVM-rbf	96.2 (1.3)	99.3 (0.0)	99.9 (0.0)	99.1 (0.8)	73.4 (27.1)
kNN	96.3 (1.8)	99.3 (0.0)	99.4 (0.5)	98.9 (0.8)	82.5 (30.7)
RFC	95.5 (2.2)	99.0 (0.0)	100.0 (0.0)	98.8 (1.9)	86.4 (30.6)

According to our observations, not only the gyr$_v$ signal, but also the gyr$_{ap}$ signal and a combination of the aforementioned (gyr$_{comb}$) are alternating in a gait sequence with respect to the left and right ICs (Fig. 1). Our results indicate that there are different favorable input signals for different sub data sets, reflecting that different gait impairments exist depending on the respective health condition [18]. This is a valuable extension of the work of McCamley et al., who used only data from young and healthy participants. As the accuracy depends on the clinical population, an a-priori decision per subject for the input signal axis is required (Table II).

The use of ML models allows the simultaneous application of multiple features as input for the binary classification. Besides the signal values, also the values of the first and second derivative at the IC time points were used in our experiments and two different sensor axes were exploited,

Authorized licensed use limited to: Norges Teknisk-Naturvitenskapelige Universitet. Downloaded on July 14,2022 at 10:45:38 UTC from IEEE Xplore. Restrictions apply.

resulting in a six-dimensional feature space. The pair plots underline that even if gyroscope data was not separable by means of just the sign of the filtered raw signal, it was possible to separate the classes when using multiple features and sensor axes (Fig. 2). Further visual inspection of pair plots revealed distinct inter-participant differences regarding the separability of the classes by either the gyr_v or the gyr_{ap} data on their own. Using a feature vector with different features from the gyr_v and the gyr_{ap} axes automatically provides a signal combination, that is more valuable for the classification than selecting only one of the gyroscope axes a-priori (like in the McCamley algorithm) or computing a hand-crafted signal combination like gyr_{comb}.

The performance of the ML approaches can be described as superior compared to the algorithm by McCamley et al. (Table II, Fig. 3). Within each subgroup, the different ML approaches achieved similar accuracy values, indicating that not a specific model, but the separability of the data in higher dimensional space was responsible for the improvements compared to the algorithm by McCamley et al. (Table II). Furthermore, there was no tendency that the group specific models performed better than the model trained on all data, which hints to a good generalizability over clinical populations.

Although the results indicate that the use of ML models for the distinction of left and right ICs is very promising, a limitation of this study is that the time points of the ICs were not derived from a dedicated IMU algorithm, but from an external reference system. Even though the instrumented mat is an accepted gold standard system for gait analysis, it could be possible that the IC time points have an offset compared to the results of a usual IC detection algorithm for IMU signals. However, for this study, the isolation of the task of left-right distinction was desired and the specific origin of the reference ICs can be considered irrelevant for the presented results.

Furthermore, we evaluated the algorithms on an in-lab data set that was heterogeneous regarding the study population but not with respect to the gait movements. It can be expected that the classification will be more challenging for gait movements from real-life scenarios including curvilinear and inclined walking, as well as spurious, unsteady gait bouts.

Hence, in future investigations, the experiments should be extended by assigning ICs detected by an actual IMU-based algorithm. Additionally, a validation on real-world data would be desirable in order to estimate the robustness of the algorithm on signals measured in challenging setups. In this context, an adaptation of the filters during preprocessing and an extension of the feature set should also be considered.

To conclude, our study showed that the optimal sensor axis for the distinction of left and right ICs with the algorithm of McCamley et al. was affected by the investigated study population. Even higher accuracy was achieved by applying ML algorithms with six-dimensional input data. Our results will contribute to a reliable stride-based gait analysis using inertial data measured at the lower back and thus support clinical decisions in the context of movement disorders.

ACKNOWLEDGMENT

This project has received funding from the Innovative Medicines Initiative 2 Joint Undertaking under grant agreement No 820820. This Joint Undertaking receives support from the European Unions Horizon 2020 research and innovation programme and EFPIA. B. M. Eskofier gratefully acknowledges the support of the German Research Foundation (DFG) within the framework of the Heisenberg professorship programme (grant number ES 434/8-1). The authors would like to thank Silvia Del Din for her input during the discussions about this study.

REFERENCES

[1] L. Rochester *et al.*, "A roadmap to inform development, validation and approval of digital mobility outcomes: the mobilise-d approach," *Digital Biomarkers*, vol. 4, no. 1, pp. 13–27, 2020.

[2] J. C. Schlachetzki *et al.*, "Wearable sensors objectively measure gait parameters in parkinsons disease," *PloS one*, vol. 12, no. 10, p. e0183989, 2017.

[3] H. Gaßner *et al.*, "Gait variability as digital biomarker of disease severity in huntingtons disease," *Journal of neurology*, pp. 1–8, 2020.

[4] A. Mannini *et al.*, "A machine learning framework for gait classification using inertial sensors: Application to elderly, post-stroke and huntingtons disease patients," *Sensors*, vol. 16, no. 1, p. 134, 2016.

[5] M. W. Whittle, "Chapter 2 - normal gait," in *Gait Analysis (Fourth Edition)*, fourth edition ed., M. W. Whittle, Ed. Edinburgh: Butterworth-Heinemann, 2007, pp. 47 – 100. [Online]. Available: http://www.sciencedirect.com/science/article/pii/B9780750688833500076

[6] M. A. Roos *et al.*, "The structure of walking activity in people after stroke compared with older adults without disability: a cross-sectional study," *Physical therapy*, vol. 92, no. 9, pp. 1141–1147, 2012.

[7] F. Kluge *et al.*, "Consensus based framework for digital mobility monitoring," *medRxiv*, 2020.

[8] J. M. Hausdorff, "Gait variability: methods, modeling and meaning," *Journal of neuroengineering and rehabilitation*, vol. 2, no. 1, pp. 1–9, 2005.

[9] G. Yogev *et al.*, "Gait asymmetry in patients with parkinsons disease and elderly fallers: when does the bilateral coordination of gait require attention?" *Experimental brain research*, vol. 177, no. 3, pp. 336–346, 2007.

[10] L. Brognara *et al.*, "Assessing gait in parkinsons disease using wearable motion sensors: a systematic review," *Diseases*, vol. 7, no. 1, p. 18, 2019.

[11] J. McCamley *et al.*, "An enhanced estimate of initial contact and final contact instants of time using lower trunk inertial sensor data," *Gait & posture*, vol. 36, no. 2, pp. 316–318, 2012.

[12] M. E. Micó-Amigo *et al.*, "A novel accelerometry-based algorithm for the detection of step durations over short episodes of gait in healthy elderly," *Journal of NeuroEngineering and Rehabilitation*, vol. 13, no. 1, pp. 1–12, 2016.

[13] A. Paraschiv-Ionescu *et al.*, "Locomotion and cadence detection using a single trunk-fixed accelerometer: validity for children with cerebral palsy in daily life-like conditions," *Journal of neuroengineering and rehabilitation*, vol. 16, no. 1, p. 24, 2019.

[14] M. Tietsch *et al.*, "Robust step detection from different waist-worn sensor positions: Implications for clinical studies," *Digital biomarkers*, vol. 4, no. 1, pp. 50–58, 2020.

[15] D. Trojaniello *et al.*, "Estimation of step-by-step spatio-temporal parameters of normal and impaired gait using shank-mounted magneto-inertial sensors: application to elderly, hemiparetic, parkinsonian and choreic gait," *Journal of neuroengineering and rehabilitation*, vol. 11, no. 1, p. 152, 2014.

[16] F. Pedregosa *et al.*, "Scikit-learn: Machine learning in Python," *Journal of Machine Learning Research*, vol. 12, pp. 2825–2830, 2011.

[17] L. Abel *et al.*, "Classification of acute stress-induced response patterns," in *Proceedings of the 13th EAI International Conference on Pervasive Computing Technologies for Healthcare*, 2019, pp. 366–370.

[18] W. Pirker and R. Katzenschlager, "Gait disorders in adults and the elderly," *Wiener Klinische Wochenschrift*, vol. 129, no. 3-4, pp. 81–95, 2017.

Authorized licensed use limited to: Norges Teknisk-Naturvitenskapelige Universitet. Downloaded on July 14,2022 at 10:45:38 UTC from IEEE Xplore. Restrictions apply.